The HINS Linac Shielding Assessment

Peter Kasper

December 28, 2010

Fermi National Accelerator Laboratory

1 Introduction

The High Intensity Neutrino Source (HINS) R&D program will investigate and demonstrate accelerator technology that might find application in a high energy, high intensity, superconducting linac suitable to serve the next generation of neutrino physics experiments or muon storage ring or collider R&D. The scope of this program includes operation of a high power klystron RF power source, testing high power RF control components, testing conventional and superconducting accelerating cavities, and construction of a low energy linear accelerator (linac) capable of accelerating protons or H^- ions up to 10 MeV.

This shielding assessment evaluates the HINS linac radiation shielding to ensure that it meets the standards set forth in the "Fermilab Radiological Control Manual" (FRCM). To the extent possible, it has been produced in accordance with Accelerator Division Procedure ADSP-02-0110. However, due to the HINS linac's low and variable beam energies, its relatively small size, and the fact that it is entirely above ground, this facility does not easily fit into the shielding assessment model used for most other Fermilab accelerators and beam lines and assumed in the procedure. In what follows, we describe how this assessment differs from the outline presented in ADSP-02-0110.

The scaling rules used to define the "Shielding Requirements" mentioned in ADSP-02-0110 are only applicable at energies above 1 GeV and break down entirely in the energy range relevant to the HINS linac. Therefore we have used more appropriate energy scaling formulae to determine source terms and attenuation factors. These are described in detail in sections **3.3** and **3.4**.

As a consequence of the small size and rapidly changing beam energy with respect to position along the beam line, there is no obvious relation between loss location and dose rate at any point outside the location. This means that the Longitudinal and Transverse shielding summaries requested in ADSP-02-0110 are not particularly meaningful for this facility. It also means that the areas outside the HINS linac cannot be classified in terms of the standard Cossairt categories defined in reference [5]. Thus we are unable to produce a spreadsheet defining "Shielding Requirements" as requested in the Accelerator Division procedure, ADSP-02-0110.

In lieu of the incremental shielding methodology this assessment uses a "brute force" approach to assessing the linac's prompt radiation shielding. Rather than assuming a generic source term for each shielding element, we calculate the expected dose rates from all possible loss points.

Since the mass of a muon is 106 MeV, it is not possible to produce them with a 10 MeV beam. Hence we have not included a section on muon production rates.

2 Site Description

The HINS linac will be installed and operated inside a concrete enclosure in the Meson Detector Building. Layouts of the enclosure are shown in Figure 1 and Figure 2. It consists of two sections; the “Ion Source and RFQ Area”, and the “Linac Area”. The “Ion Source and RFQ Area” will contain a 50 KeV proton or H^- ion source, a Radio Frequency Quadrupole (RFQ) accelerator, and support equipment sufficient to generate a 2.5 MeV beam at currents up to approximately 25 mA at a 1% duty cycle. As documented in [2], all radiation hazards, associated with the RFQ and 2.5 MeV beam, have already been assessed and the design and operation of those components have been found to be compliant with FRCM requirements.

The “Linac Area” will house the linac accelerator and beam line components. This will include both conventional copper and superconducting accelerating cavities, superconducting solenoids for beam focusing, beam absorbers, and any necessary support equipment that is most appropriately located within the beam enclosure. Ancillary power supplies, controls and diagnostics equipment, and other accelerator support equipment will be located outside the enclosure.

The enclosure itself is built with overlapping, prefabricated concrete shielding blocks. During the construction of the enclosure, care was taken to avoid leaving gaps larger than 0.25 inches between the blocks. Where this was not possible, the gaps were filled with sand or grout.

Access to the enclosure is achieved via three concrete labyrinths that are located at the upstream and downstream ends and along the west side wall. There are also several penetrations for routing the pipes and cables needed to cool, power, and operate the equipment inside. The expected beam line layouts are shown in Figure 1 and the labyrinths and penetrations are identified in Figure 1 and Figure 2 respectively.

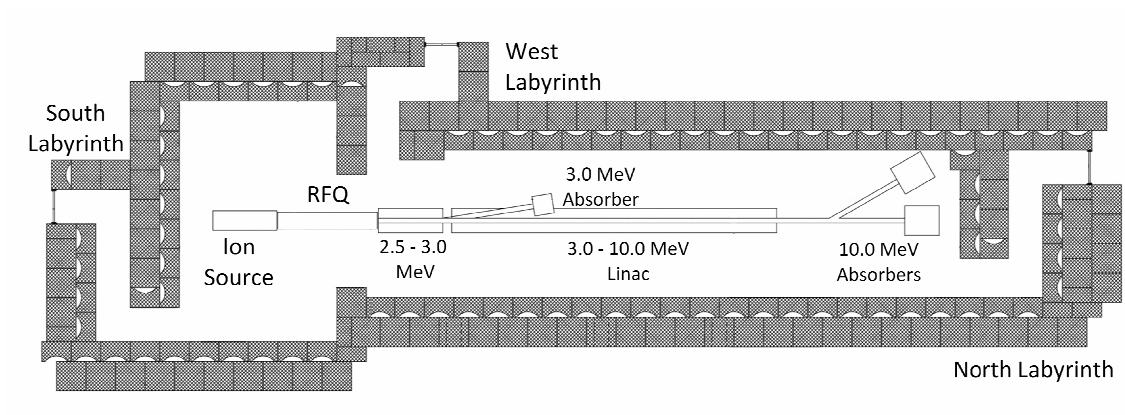

Figure 1: Plan view of the HINS linac showing the access labyrinths and three beam line configurations.

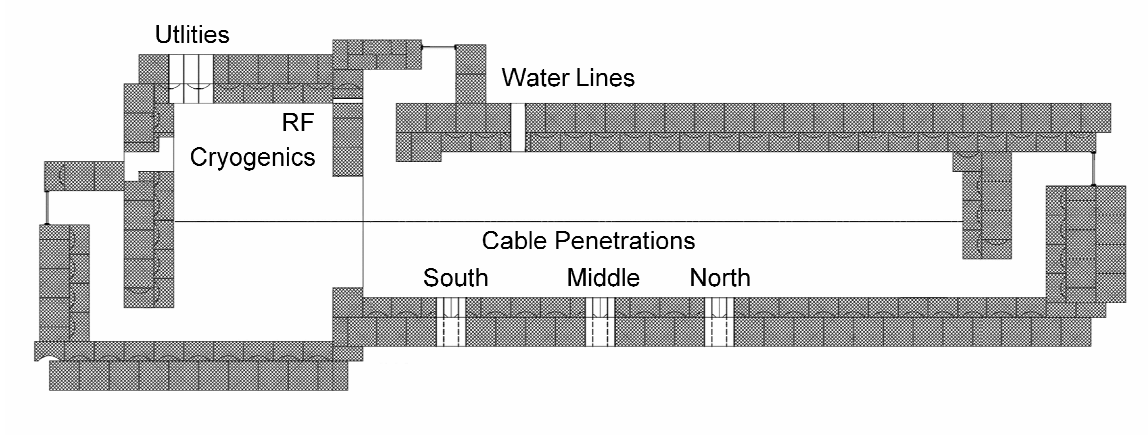

Figure 2: Plan view of the HINS linac enclosure showing the locations of the various penetrations.

3 Assessment Parameters and Methodology

In this section we describe the various parameters, equations, and methods used in the assessment. The locations of loss points and the various labyrinths and penetrations will be referenced with respect to the accelerator axis line. This line will define our z-axis and its origin will be assumed to be at the start of the linac section of the enclosure; 19 ft from the inside face of the south wall. The positive y-axis will be assumed to point horizontally to the west, while the x-axis measures heights above the beam. The y and z axes are shown in Figure 2. Large scale drawings of the enclosure, included as attatchments (Dwgs. 481766 and 481767) indicate all the dimensions relevant to this assessment.

In subsection **3.1** we present the assumed beam power that the linac enclosure is designed to shield. Subsection **3.2** describes the assumptions made concerning both normal operating conditions and all potential accident conditions.

Most other shielding assessments produced at Fermilab deal with particle beams at energies well above 1 GeV. The energy scaling formulae used in those assessments do not extrapolate correctly into the energy range relevant to this analysis and have been replaced with more appropriate ones. In subsection **3.3** we introduce the formula used to predict the prompt radiation dose rates generated by proton beams in the energy range of 3 to 10 MeV and in subsection **3.4** we present the energy dependent radiation attenuation lengths that are used in determining how much radiation can propagate through concrete shielding.

3.1 Beam Power

The ion source and RFQ accelerator are capable of producing a beam current of 25 mA with a 1% duty factor and a maximum pulse length of 3 msec. This corresponds to 4.7E14 protons or H^- ions per pulse at 3.33 Hz. Though shorter pulses can be delivered at higher rep rates the overall beam power is limited to 1.56E15 protons per second (5.6E18 p/hr) at a maximum energy of 10 MeV. This corresponds to 750W at 3 MeV and 2.5 KW at 10 MeV.

This assessment will evaluate the enclosure shielding with respect to this maximal beam power even though the normal operating conditions are expected to be at much lower intensities.

It is expected that on average, the machine will operate at less than half its maximum capacity for no more than 6 hrs a day and 720 hrs a year. This corresponds to 2.0E21 protons per year.

3.2 Normal and Accident Conditions

The Fermilab Radiological Control Manual (FRCM 2.3, 2010) describes the posting criteria and the controls for Fermilab accelerator areas for different radiological conditions. In Table 1 we identify the different parts of the HINS facility that will be subject to those requirements, and indicate the dose limits that pertain to each area under both normal and accident conditions.

Area	Control Type	Maximum Normal Dose Rate (mrem/hr)	Maximum Accident Dose (mrem)
Inside Enclosure	High Radiation Area No Beam-on Access	> 100	>500
Roof of Enclosure and Labyrinths	Minimal Occupancy Controlled Area	0.25 to 5	< 10
Outside Enclosure above 10.5 ft.	Minimal Occupancy Controlled Area	0.25 to 5	< 10
Outside Enclosure at Floor Level	Unlimited Occupancy Controlled area	< 0.25	< 5

Table 1: HINS linac radiation control areas and allowed dose rate limits as described in FRCM, 2.3 [6].

Four beam line configurations are considered in this assessment. They differ in the location of the beam absorber (on-axis or off-axis) and the maximum available beam energy (10 MeV or 3 MeV). Figure 1 shows the location of the absorber for three of

them. The two 10 MeV modes differ in the position of the absorber. In the on-axis case there are no bending elements in the beam while the off-axis case has a single bend used for spectral measurements. Similarly, there will also be two 3 MeV modes; the one shown has the beam absorber in an off-axis position, while the other mode has it on-axis at about the same distance from the start of the linac. Table 2 lists the absorber locations used in this assessment.

The center lines for all four beams are 50.6 inches above the enclosure floor.

	z-location (ft)	y-location (ft)
3 MeV off-axis	**18**	**3**
3 MeV on-axis	**18**	**0**
10 MeV off-axis	**56**	**6**
10 MeV on-axis	**56**	**0**

Table 2: Location of the beam absorber for each of the four operating configurations.

3.2.1 Normal Operating Conditions

Under normal operating conditions the beam will be transported through vacuum filled beam pipes into a shielded beam absorber illustrated in Figure 3. Calculations done for normal running conditions will assume that all radiation is produced inside the beam absorber and is attenuated by the absorber's shielding.

The absorber itself consists of a water-cooled, conical, nickel target mounted inside a steel box with 4 inch thick walls. The space between the steel and the target will be packed with polyethylene beads and the steel box itself will be encased in 6 inch thick blocks of polyethylene.

The attenuation provided by the absorber was determined using Mars simulations of the absorber with and without polyethylene [3]. The calculations were performed for 5.6E18 protons/hr at both 3 MeV and 10 MeV energies.

For the 10 MeV case with no polyethylene Mars predicted the dose rate on the outer surface of the steel box, 1 foot from the point of impact, to be 7.00E5 mrem/hr. It also attributed an attenuation factor of 30 to the steel box. A simulation with the complete absorber configuration predicted a dose rate of 4.13E3 mrem/hr on the outer surface of the polyethylene casing; 1.5 ft from the point of impact. We can use these results to deduce that attenuation factor provided by the absorber.

- Dose rate at 12" after 4" of steel and no polyethylene filler: $Ds^{R=12}$ = 7.00E5
- Dose rate at 18" after both steel and polyethylene shielding: $Dsp^{R=18}$ = 4.13E3

- Dose rate at 8” from the target with no shielding: $D^{R=8} = 30 \times Ds^{R=12} = 2.10E7$
- Dose rate at 18” from the target with no shielding: $D^{R=18} = (8/18)^2 \times D^{R=8} = 4.15E6$
- Absorber attenuation factor: $A = D^{R=18} / Dsp^{R=18} = 4.13E3 / 4.15E6 = 1.00E3$

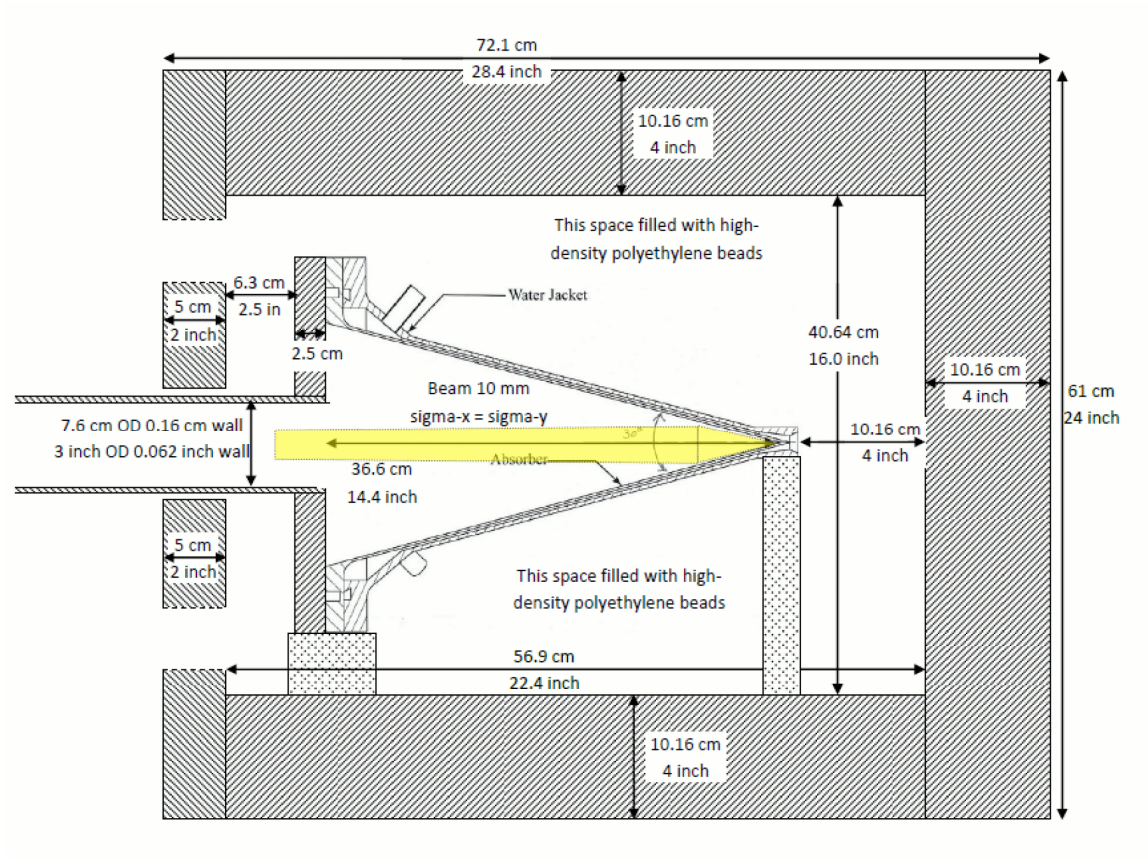

Figure 3: HINS beam absorber. The structure shown above will be encased in a 6 inch thick polyethylene envelope.

For the 3 MeV case the simulated neutron production rate on this target was so low that dose rates could not be measured.

When calculating dose rates from normal operating conditions we could simply use the source term form the MARS simulations. However this result is specific to the simulated target material and the energy scaling is undefined. In order to calculate doses at other energies, we have defined a parametric source term (see section 3.3). At 10 MeV the parametric source term predicts a dose rate of 1.21E+07 mrem/hr at 1 ft from the interaction point and 90 degrees with respect to the beam direction. For comparison, the corresponding MARS value is 0.93E+07 mrem/hr.

For the sake of consistency, we shall uses the parametric source term in both normal and accident calculations. For normal conditions we shall apply the absorber attenuation factor deduced above to both 3 MeV and 10 MeV beam line configurations.

3.2.2 Accident Conditions

We define an accident condition as any 3 to 10 MeV beam loss that occurs outside the beam absorber. The material of the vacuum pipe constrains the location of loss points to lie along the beam line connecting the RFQ and the beam absorber. The various RF cavities that accelerate the beam take up space in the beam line and consequently limit the locations where the higher energy beam can interact. In this assessment we assume that the beam reaches 3 MeV at z = 7.0 ft. For 10 MeV configurations, the acceleration from 3 to 10 MeV is assumed to start at z = 7.5 ft and reach 10 MeV at z = 42 ft. The energy is assumed to rise linearly over this range.

The three absorber configurations shown in Figure 1 and detailed below are included when assessing loss points.

1. The absorber is located approximately 3 ft west of the z-axis and 18 ft along it. The bend point is assumed to be located 8 ft along the axis line. In this configuration the beam energy is limited to 3 MeV.

2. The absorber is located approximately 6 ft west of the z-axis and 56 ft along it. The bend point is located at z = 48 ft and the beam energy ranges from 3 to 10 MeV.

3. The absorber is located on the beam axis at z = 56 ft. In this configuration there is no bend point and the beam energy ranges from 3 to 10 MeV.

The on-axis 3 MeV case is not explicitly addressed, since a loss generated at the same location while in a 10 MeV beam configuration will have the same maximum intensity but will occur at a higher energy and hence will always be worse.

When presenting doses caused by accident conditions we will always choose the worst case scenario. That is we will assume that the loss involves the full beam intensity at the highest possible energy, and at a location that maximizes the generated dose rate.

We shall also assume that interlocked radiation detectors will detect the loss and trip off the beam, thereby limiting its duration. Since these detectors have a one second response time, we will assume that up to 3 beam pulses or 1.56E15 protons can be lost during an accident. Furthermore for each calculation we shall choose the loss point that maximizes the dose generated.

3.3 Low Energy Source Term

Most shielding assessments done at Fermilab assume that the radiation produced by proton beams scales as $E^{0.8}$, where E is the proton energy. This however, is only valid at high energies and significantly overestimates the dose rate at energies of a few MeV. To estimate the amount of radiation produced by the HINS proton beam we start with the source term parameterization given in equation (1).

$$S(E,r,\theta_s) = 2\times 10^{-5}(1+E^{0.6})\left(1-e^{-3.6E^{1.6}}\right)/\left(0.3048\, r\left(\theta_s + 40/\sqrt{E}\right)\right)^2$$

Equation 1: Dose in mrem per proton at a distance r ft from the loss point and at an angle of θ_s degrees with respect to the beam direction. The proton energy E is measured in units of GeV.

This expression is a parameterization published in reference [4] that is valid for proton energies below one GeV, and that describes neutron production near threshold.

$$f(R,D) = \cos[\tan^{-1}\left(\frac{D}{R}\right)]$$

Equation 2: Geometric correction factor used in calculating dose rates from neutrons propagating through labyrinths and penetrations.

When calculating the dose rate propagating through a labyrinth or penetration the orientation of the opening with respect to the loss point must also be taken into account. This geometric correction is given in Equation 2 and is expressed in terms of two distance variables R and D (see Figure 4). R is defined as the perpendicular distance from the loss point to the plane orthogonal to the opening and D is the offset distance such that $\sqrt{R^2+D^2}$ is the straight line distance from the loss point to the opening.

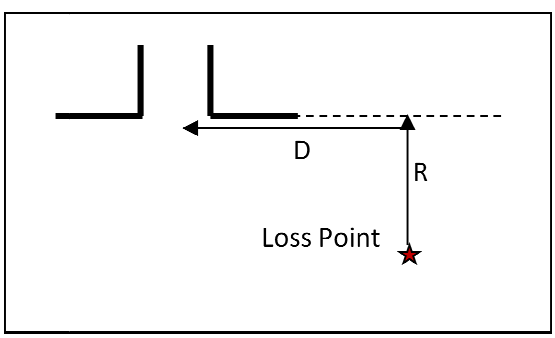

Figure 4: Definition of the R and D distances used in labyrinth and penetration calculations.

3.4 Concrete Attenuation Lengths at Low Energy

For neutron energies below 100 MeV the attenuation length in concrete is significantly shorter than what is normally assumed in shielding assessments at Fermilab. The mean free path of low energy neutrons relative to the high energy asymptote has been parameterized [4] as shown in Equation 3.

$$\frac{\lambda_{LE}}{\lambda_{\mathrm{HE}}} = 1 - 0.8\,\mathrm{e}^{-5.\mathrm{E}}$$

Equation 3: The energy dependence of the mean free path for neutrons passing through concrete given as a ratio with respect to its high energy asymptote value, λ_{HE}. E is in units of GeV.

At high energy, 3 ft of concrete is required in order to obtain a factor of 10 reduction in dose rate. Thus we can use the formula above to obtain an energy dependent expression for the attenuation provided by T_{conc} feet of concrete. The resulting formula is given in Equation 4.

$$A(E) = 10^{\frac{-T_{conc}}{3}/\left(1 - 0.8\,e^{-5.E}\right)}$$

Equation 4: The amount by which neutron radiation is reduced after passing through T_{conc} feet of concrete. E is the neutron energy in GeV.

In the dose rate calculations presented in the following sections we take E to be equal to the beam energy. This simplification is conservative in that the real neutron energies are necessarily lower and hence we will be underestimating the amount of attenuation provided by the concrete shielding.

4 Prompt Radiation Shielding

In this section we detail the calculations that have been done to assess the linac enclosure's conformance with the FRCM limits listed in Table 1. The calculations assess the shielding provided by the enclosures walls and roof, and determine the amount of radiation that can leak out of the enclosure by way of the various labyrinths and penetrations. Table 3 summarizes the results.

	Normal Operations (mrem/hr)	FRCM Limit (mrem/hr)	Accident Dose mrem	FRCM Limit mrem
Walls	**5.49E-03**	**0.25**	**1.53E-03**	**5.0**
Roof	**0.02**	**5.0**	**5.58E-03**	**10**
South Labyrinth	**1.37E-03**	**0.25**	**4.85E-04**	**5.0**
West Labyrinth	**8.52E-04**	**0.25**	**2.51E-03**	**5.0**
North Labyrinth	**0.074**	**0.25**	**0.021**	**5.0**
South Cable Penetration	**2.05E-03**	**0.25**	**3.33E-03**	**5.0**
Middle Cable Penetration	**3.32-03**	**0.25**	**0.012**	**5.0**
North Cable Penetration	**9.41-03**	**0.25**	**0.032**	**5.0**
Water Lines: 50% Full (empty)	**0.215 (0.358)**	**0.25**	**0.216 (0.360)**	**5.0**
Utilities Penetration	**0.063**	**0.25**	**0.032**	**5.0**
Cryogenics Penetration	**0.135**	**0.25**	**0.050**	**5.0**
RF Penetration	**1.60E-3**	**5.0**	**1.23E-03**	**10**

Table 3: Summary of the maximum dose rates found for both normal running and accident conditions.

The dose rates given in Table 3 are the highest obtained from the four beam configurations shown in Figure 1 and defined in Table 2. In all cases, we assume the maximum possible beam intensity, 5.60E+18 protons/hr, and an absorber attenuation factor of 1.00E+03. Table 4 lists the source term parameters that produced the particular dose rates listed in Table 3.

	Beam Condition	E (MeV)	R (ft)	D (ft)	Θ_s (degrees)	Source Term (mrem/s)
South Labyrinth	Normal	10.00	75.00	16.58	155.6	4.31E-04
	Accident	10.00	61.00	10.58	170.2	6.39E-01
West Labyrinth	Normal	3.00	6.17	16.25	159.2	1.69E-04
	Accident	3.00	6.17	5.25	130.4	1.79E+00
North Labyrinth	Normal	10.00	4.50	5.83	52.4	4.42E-02
	Accident	10.00	4.50	5.83	52.4	4.44E+01
South Cable Penetration	Normal	3.00	7.83	9.64	136.4	6.18E-04
	Accident	4.09	7.83	5.20	114.4	3.25E+00
Middle Cable Penetration	Normal	10.00	13.83	32.19	165.4	8.09E-04
	Accident	6.68	7.83	3.83	100.7	1.42E+01
North Cable Penetration	Normal	10.00	13.83	20.30	171.6	2.30E-03
	Accident	9.06	7.83	3.73	99.2	3.06E+01
Water Lines	Normal	3.00	4.17	7.39	96.5	1.14E-03
	Accident	5.28	7.17	7.65	106.7	4.12E+00
Utilities Penetration	Normal	10.00	12.17	73.87	169.7	7.18E-05
	Accident	9.26	12.17	56.30	166.6	1.34E-01
Cryogenics Penetration	Normal	10.00	75.00	7.04	142.7	4.79E-04
	Accident	10.00	61.00	9.35	171.3	6.42E-01
RF Penetration	Normal	10.00	4.67	67.00	176.0	3.73E-05
	Accident	3.00	4.67	18.00	165.5	1.03E-01

Table 4: Input parameters used to define the source term used in the labyrinth and penetration calculations for the worst case accident.

The only result that exceeded the corresponding FRCM limit was from the 3.0 MeV normal operating configurations. In these modes the dose rate at the outside opening of the straight penetration that brings water lines into the enclosure was calculated to be 0.36 mrem/hr (off-axis) and 0.34 mrem/hr (on-axis). The calculation assumed the 1.5 x 1.5 ft opening to be completely empty. In practice it will be packed with sandbags in order to reduce the effective size of the opening. Conservatively assuming that the

opening was only 50% filled, we repeated the calculation and found that this was sufficient to bring the dose rate down below the 0.25 mrem/hr limit. It should also be noted that the absorber attenuation factor used, was derived from a 10 MeV simulation and therefore underestimates the attenuation at 3 MeV. In fact, the Mars simulation used to evaluate the beam absorber design predicted that no neutrons would escape the absorber with a 3 MeV beam. If one assumes the 3 MeV dose rates are negligible, then the maximum dose rate will be 0.08 mrem/hr from the on-axis 10 MeV configuration.

The accident condition doses listed in Table 3, all assume the use of interlocked radiation detectors to limit the loss duration to one second. The doses are derived from the worst case accident condition for each labyrinth or penetration. These were obtained by varying the assumed loss point along the beam line for each of the target locations and choosing the location and energy combination that produced the highest dose rates.

The highest one second dose that was found occurs when beam is lost inside the linac where it passes by the water line penetration. For the 10 MeV configurations the beam energy has reached 5.3 MeV at that location. The dose expected from this accident is estimated to be 0.36 mrem when we assume the penetration to be empty. This is well below the 5 mrem per accident limit.

The subsections that follow describe in more detail, the calculations that were done in order to produce the results listed in Table 3 and Table 4.

4.1 Wall and Roof Shielding

The enclosure is constructed out of concrete shielding blocks as shown in Figure 2. The side walls are composed of overlapping layers of B blocks and Q blocks. In plan view, the B blocks are 3 ft square while the thickness of the Q blocks varies from 2 ft at the ends to 1.5 ft in the middle. Thus the walls provide from 4.5 ft to 5 ft of shielding, however, for simplicity's sake we shall make the conservative assumption that the walls only provide 4.5 ft of shielding.

The maximum dose that could be received by persons outside the enclosure occurs where the 10 MeV beam enters the off-axis beam absorber. At this location the beam is not only at its maximum energy, but is also at its shortest distance to the enclosure walls.

With the input parameters listed in Table 4, Equation 1 (defined in subsection **3.3**) is used to calculate the dose rate just inside the enclosure wall nearest to the loss point. For normal running we apply the absorber attenuation factor obtained in subsection **3.2.1**, while for the accident condition we assume a one second beam loss. The dose rate outside the enclosure is then obtained by applying an attenuation factor obtained with Equation 4 assuming 4.5 ft of concrete and a neutron energy equal to the beam energy.

The wall shielding calculation is summarized in Table 5 For normal operations the dose rate is 0.005 mrem/hr; well below the 0.25 mrem/hr limit. The one second dose under

accident conditions is also well below the limit of 5 mrem per accident. Thus we conclude that the enclosure wall thickness is adequate for the expected beam energies and intensities.

Energy, E (GeV)	**10.0**	**Protons/hr**	**5.60E+18**
Distance to wall (ft)	**1.17**	**θ_s (deg)**	**53**
R (ft)	**1.17**	**D (ft)**	**0.0**

	Normal (mrem/hr)	**Accident (mrem)**
Dose at inside wall	**1.04E+04**	**2.89E+03**
Dose after 4.5 ft of shielding	**5.49E-03**	**1.53E-03**

Table 5: Calculation of the maximum dose rate expected outside the enclosure walls

Energy, E (GeV)	**10.0**	**Protons/hr**	**5.60E+18**
Distance to ceiling (ft)	**6.3**	**θ_s (deg)**	**90**
R (ft)	**6.3**	**D (ft)**	**0.0**

	Normal (mrem/hr)	**Accident (mrem)**
Dose at ceiling	**3.05E+02**	**8.52E+01**
Dose after 3.0 ft of shielding	**2.00E-02**	**5.58E-03**

Table 6: Calculation of the maximum dose rate expected on the enclosure roof.

At its lowest point the roof of the enclosure in the Linac region is 10.5 feet above the floor and 6.3 ft above the beam line. It consists of two overlapping layers of 1.5 ft thick concrete shielding blocks that provide a total of 3.0 ft of shielding. Table 6 summarizes the calculation of the expected dose rates on the enclosure roof directly above a 10 MeV beam loss.

For normal operations the dose rate is 0.02 mrem/hr; well below the 5.0 mrem/hr limit for a minimal occupancy area. The one-second dose under accident conditions is also well

below the limit of 10 mrem per accident. Thus we conclude that the enclosure roof thickness is adequate for the expected beam energies and intensities.

4.2 Access Labyrinths

Personnel access to the enclosure is provided by three labyrinths. The south labyrinth is built into the south wall of the Ion Source & RFQ area. The west labyrinth is built into the west wall of the enclosure adjacent to the 3 MeV end of the linac. The north labyrinth is at the 10 MeV end of the linac and is built into the north wall of the enclosure.

All access labyrinths have three orthogonal legs and have interlocked gates at the outside end of the third leg. The lengths and cross-sectional areas of the legs are shown in Table 7.

To calculate the dose rates from neutrons scattering through the labyrinths we use the standard methodology as described in TM-1834 [1]. This methodology is implemented through a spreadsheet that uses the low energy source term described in subsection **3.3**, to determine the amount of radiation at the inside face of the labyrinth. This is then propagated through each leg, taking into account its length, cross sectional area and orientation w.r.t. to the previous leg.

	South Labyrinth	West Labyrinth	North Labyrinth
1st leg length (ft.)	6.75	7.75	6.75
2nd leg length (ft.)	12.00	6.00	11.00
3rd leg length (ft.)	6.25	4.25	6.75
1st leg area (sq. ft.)	36.75	26.25	30.00
2nd leg area (sq. ft.)	36.75	26.25	26.25
3rd leg area (sq. ft.)	36.75	26.25	26.25
z-location of entrance (ft)	-19.00	1.75	60.50
y-location of entrance (ft)	-10.58	6.17	-5.83
Leg 1 short Circuit Shielding (ft)	4.5	3.0	7.5
Leg 3 short Circuit Shielding (ft)	4.5	5.0	5.0

Table 7: Dimensions and locations of the three access labyrinths.

In addition to the dose from neutrons propagating through the labyrinth or penetration we also calculate the doses expected from neutrons exiting the enclosure via “short circuit” routes. Two types of short circuits are considered and will be referred to as “Leg 1“ and “Leg 3”.

1. In a Leg 1 short circuit, neutrons that reach the end of the first leg of the labyrinth pass through the concrete shielding between there and the outside of the enclosure. To calculate the dose rates obtained through this mechanism we simply replace the attenuation factors provided by the 2nd and 3rd legs with a concrete shielding attenuation factor obtained with Equation 4 in subsection **3.4**, assuming a neutron energy equal to the beam energy.

2. In a leg 3 short circuit, neutrons pass through the concrete separating the inside of the enclosure from the start of the 3rd leg and then travel through the leg to the outside entrance. In this case the source dose is calculated at the inside wall of the enclosure adjacent to the 3rd leg entrance, the appropriate shielding attenuation is applied, and then the radiation is propagated through the 3rd leg as though it were a single leg penetration.

Target	Calculation Type	South Labyrinth	West Labyrinth	North Labyrinth
3 MeV	3-leg	2.28E-04	5.14E-04	1.71E-04
off-axis	Leg 1 Short Circuit	6.27E-09	1.30E-06	1.32E-13
	Leg 3 Short Circuit	8.21E-09	5.53E-09	1.17E-09
3 MeV	3-leg	2.52E-04	8.52E-04	1.87E-04
on-axis	Leg 1 Short Circuit	6.92E-09	2.15E-06	1.45E-13
	Leg 3 Short Circuit	8.00E-09	7.72E-09	1.17E-09
10 MeV	3-leg	1.18E-03	1.44E-05	1.16E-02
off-axis	Leg 1 Short Circuit	2.05E-07	1.24E-07	1.96E-10
	Leg 3 Short Circuit	2.16E-07	4.60E-10	1.51E-05
10 MeV	3-leg	1.16E-03	4.68E-04	7.38E-02
on-axis	Leg 1 Short Circuit	2.02E-07	4.04E-06	1.24E-09
	Leg 3 Short Circuit	2.16E-07	1.49E-08	4.48E-06

Table 8: Dose rate calculations for the access labyrinths under normal running conditions. The results are given in mrem/hr.

For normal operating conditions we performed the three calculation types for each of the four absorber locations described in subsection **3.2.2**. Table 8 lists the dose rates thus obtained.

For all three labyrinths the short-circuit calculations produced negligible dose rates. Due to its proximity, the west labyrinth is more sensitive to radiation coming from the 3 MeV

absorbers. The dose rates from the two absorber locations are comparable. However geometric effects tend to favor the on-axis configuration which produces the highest dose rate, 8.52E-04 mrem/hr.

Because it directly faces all of the absorber locations, the south labyrinth is least dependent on geometric effects. In this case the increased production from the 10 MeV beam outweighs the proximity of the 3 MeV beam absorbers. The dose rates from the two 10 MeV configurations are very similar with the off-axis configuration being slightly higher at 1.18E-03 mrem/hr.

Due to its proximity to the 10 MeV absorbers the north labyrinth is expected to see the highest dose rates with 7.38E-02 mrem/hr predicted from the on-axis configuration. This is however, well under the 2.50E-01 mrem/hr limit.

The dose rate calculations for accident conditions are performed in the same manner as for normal running conditions, but with the following differences:

1. The absorber attenuation factor is not used.
2. Instead of an hourly rate we calculate the dose obtained from a loss that persists for no more than one second. The limited duration assumes that interlocked radiation detectors have been installed in order to detect the elevated dose rates and disable the beam.
3. The 3 MeV on-axis beam line configuration is ignored because it will always produce doses that are less than or equal to those of 10 MeV beam lines at the same location.

Since we assume that an accident can occur anywhere along the beam lines, we perform the three calculation types for 100 loss points distributed along each beam line. The beam energy used in these calculations varies according to the relationship between location and energy described in subsection **3.2.2**.

The results of these calculations for the south labyrinth are presented graphically in Figure 5. We observe that the rate of increase in dose with beam energy exceeds the decrease in dose with distance. Hence worst case accident occurs when 10 MeV beam is lost at the end of the accelerating cavities. The maximum dose from a one second beam loss at this point comes from the 3-leg calculation and is 4.85E-04 mrem.

Figure 6 displays the results for the west labyrinth. In this case dose rates from the high energy loss points are strongly attenuated by both distance and solid angle effects. Consequently, the worst case accident occurs at the upstream end of the linac where the 3 MeV beam is produced. The dose resulting from a one second beam loss at that location is 2.51E-03 mrem.

The north labyrinth calculations are shown in Figure 7. All factors favor the downstream end of the on-axis 10 MeV beam line as the worst location for an accident. The one

second dose of 0.02 mrem is much higher than anything possible from either of the other two labyrinths. Nevertheless, it is still well below the 5 mrem FRCM limit.

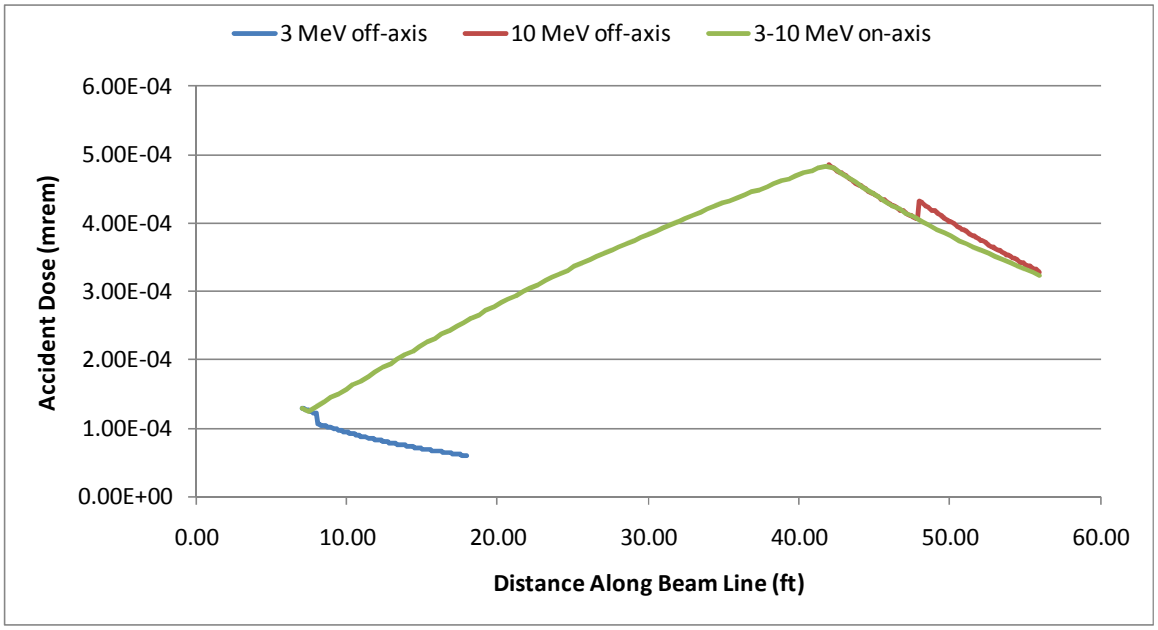

Figure 5: Maximum accident dose outside the south access labyrinth versus the location of the loss point.

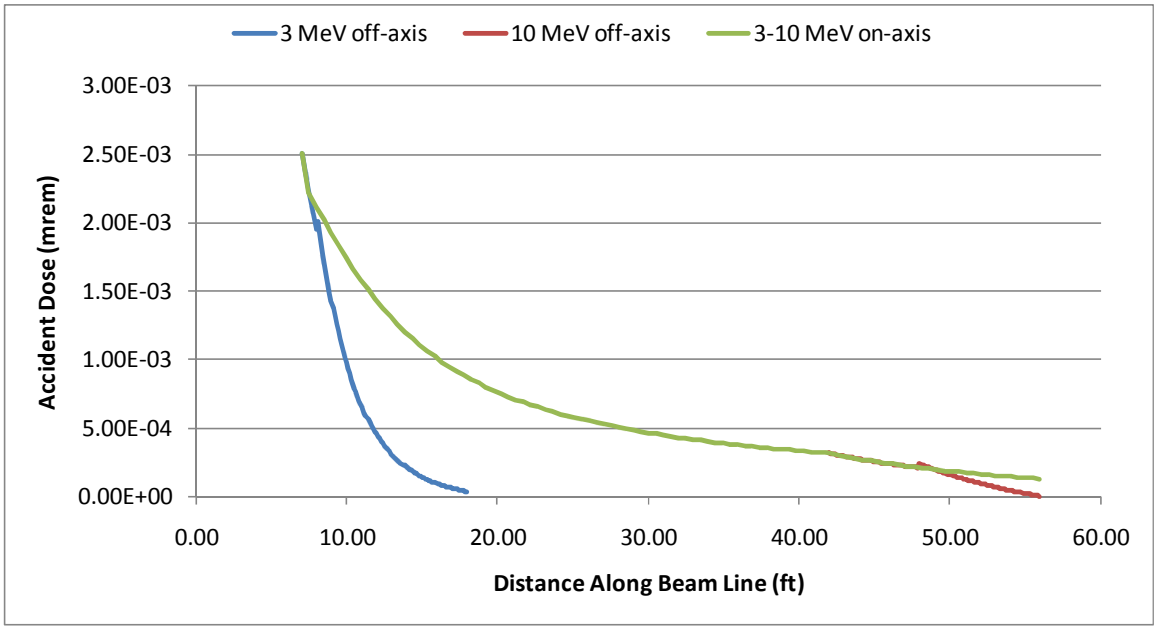

Figure 6: Maximum accident dose outside the west access labyrinth versus the location of the loss point.

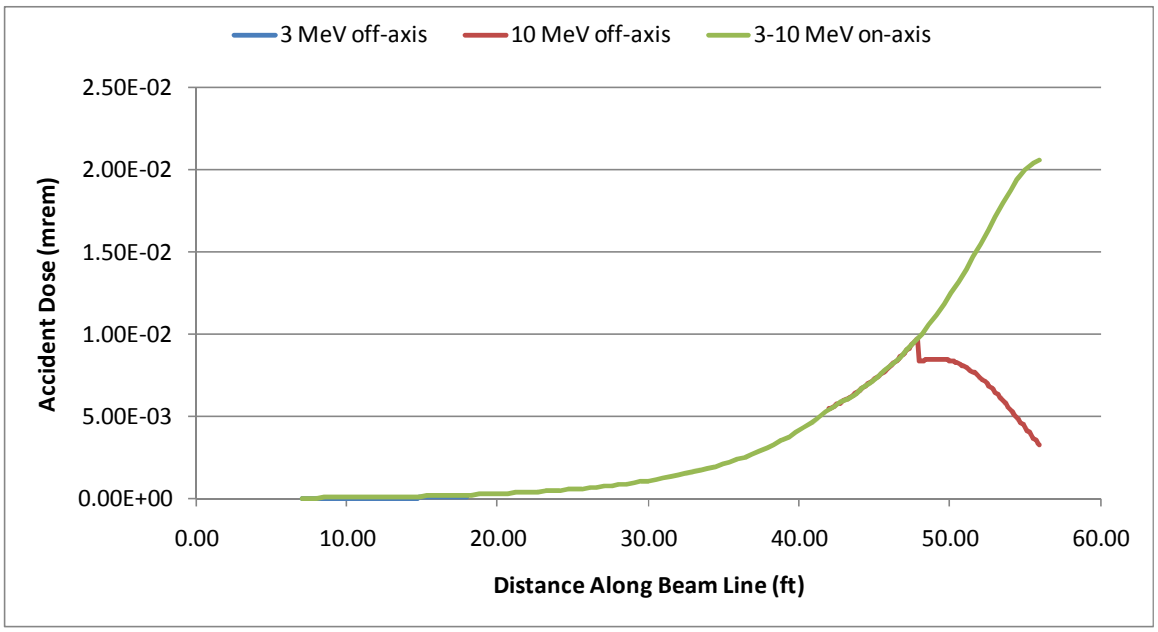

Figure 7: Maximum accident dose outside the north access labyrinth versus the location of the loss point.

4.3 East Side Cable Penetrations

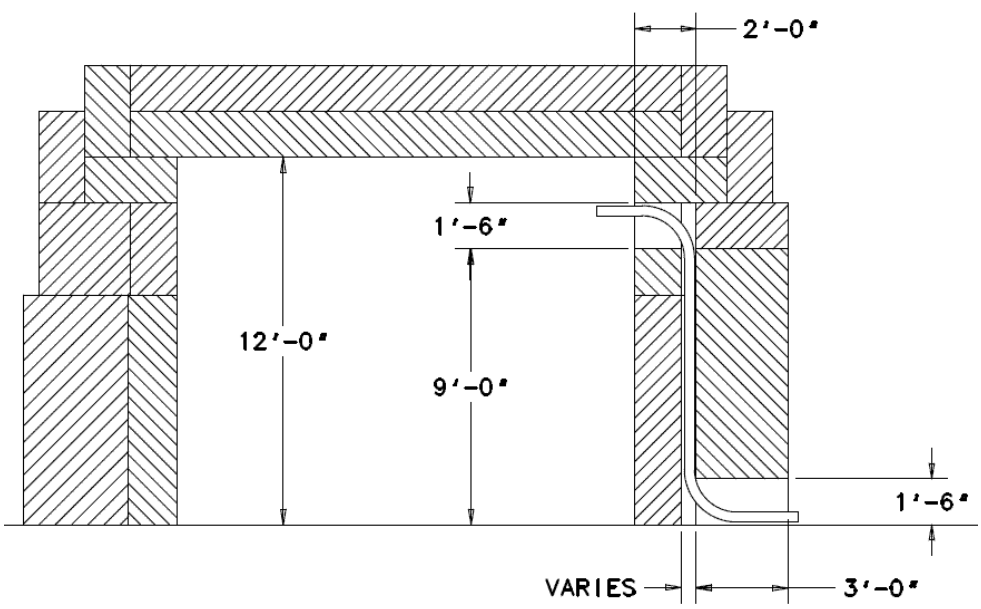

Figure 8: Elevation view of an east side wall cable penetration.

The east side wall of the enclosure contains three identical sets of cable penetrations. Each set consists of three legs. The middle leg utilizes the voids between the B-blocks

and the Q-blocks that make up the wall. The voids exist because the sides of the Q-blocks that abut the B-blocks are convex. By vertically offsetting a B-block, one allows access to two of these gaps from the top and bottom that can be used to form a 3 leg penetration for two cable conduits. Figure 8 shows an elevation view of one of these penetrations. The dose rate calculations done for these penetrations use exactly the same methodology as was used for the access labyrinths in the previous section.

The relevant dimensions of the three legs are listed in Table 9. Each opening is 9 inches wide to give a combined cross-sectional area of 1.5*(0.75+0.75) = 2.25 ft^2 for the 1st and 3rd legs. Due to the way it is created, the cross-sectional area of the 2nd leg is not clearly defined. We have therefore used a value that errs on the high side in order not to underestimate the dose rate calculations. The last row of the table indicates the amount of concrete used in the two short circuit calculations.

	South Penetration	Middle Penetration	North Penetration
1st leg length (ft.)	1.75	1.75	1.75
2nd leg length (ft.)	9.00	9.00	9.00
3rd leg length (ft.)	3.25	3.25	3.25
1st leg area (sq. ft.)	2.25	2.25	2.25
2nd leg area (sq. ft.)	1.50	1.50	1.50
3rd leg area (sq. ft.)	2.25	2.25	2.25
z-location of entrance (ft)	9.00	24.00	36.00
y-location of entrance (ft)	-7.83	-7.83	-7.83
x-location of entrance (ft)	5.53	5.53	5.53
Leg 1 short Circuit Shielding (ft)	3.0	3.0	3.0
Leg 3 short Circuit Shielding (ft)	1.5	1.5	1.5

Table 9: Dimensions and locations of the three east side cable penetrations.

For normal operating conditions we performed the dose rate calculation for each of the four absorber locations described in subsection **3.2.2**. Table 10 summarizes the calculations for the dose rate found for each penetration and beam configuration. Three calculations are presented for each penetration and beam configuration; a three-leg calculation and the two short-circuit calculations.

The doses predicted by the leg 3 short-circuit calculations are much larger than either of the other calculations. This is not surprising since the 3rd leg has only 1.5 ft of concrete

between it and the inside of the enclosure. The highest dose rate found was 0.01 mrem/hr. This rate was produced at the north cable penetration from 10 MeV beam sent into the off-axis absorber and is comfortably below the 0.25 mrem/hr limit.

Target	Calculation Type	South Cable Penetration	Middle Cable Penetration	North Cable Penetration
3 MeV	3-leg	8.77E-06	1.41E-05	3.70E-06
off-axis	Leg 1 Short Circuit	8.45E-06	1.36E-05	3.56E-06
	Leg 3 Short Circuit	1.17E-03	1.96E-03	4.65E-04
3 MeV	3-leg	9.82E-06	1.85E-05	3.42E-06
on-axis	Leg 1 Short Circuit	9.47E-06	1.79E-05	3.29E-06
	Leg 3 Short Circuit	1.37E-03	2.79E-03	4.35E-04
10 MeV	3-leg	5.57E-06	1.49E-05	4.17E-05
off-axis	Leg 1 Short Circuit	1.84E-05	4.92E-05	1.38E-04
	Leg 3 Short Circuit	1.23E-03	3.32E-03	9.41E-03
10 MeV	3-leg	3.31E-06	9.97E-06	3.52E-05
on-axis	Leg 1 Short Circuit	1.09E-05	3.29E-05	1.16E-04
	Leg 3 Short Circuit	7.29E-04	2.22E-03	8.08E-03

Table 10: Dose rate calculations for the east side cable penetrations under normal running conditions. The results are given in mrem/hr.

The calculations of accident condition doses for the cable penetrations were done in the same way used for the access labyrinths. The results are presented in Figure 9 for the south penetration, Figure 10 for the middle penetration, and Figure 11 for the north penetration. The results are much as one might expect. The highest doses are produced when losses occur close to the penetration in question and increase rapidly as the beam energy increases. The highest dose from a one second accident was found to be 0.03 mrem outside the north penetration and resulted from the leg 3 short-circuit calculation. This is well below the 5 mrem FRCM limit.

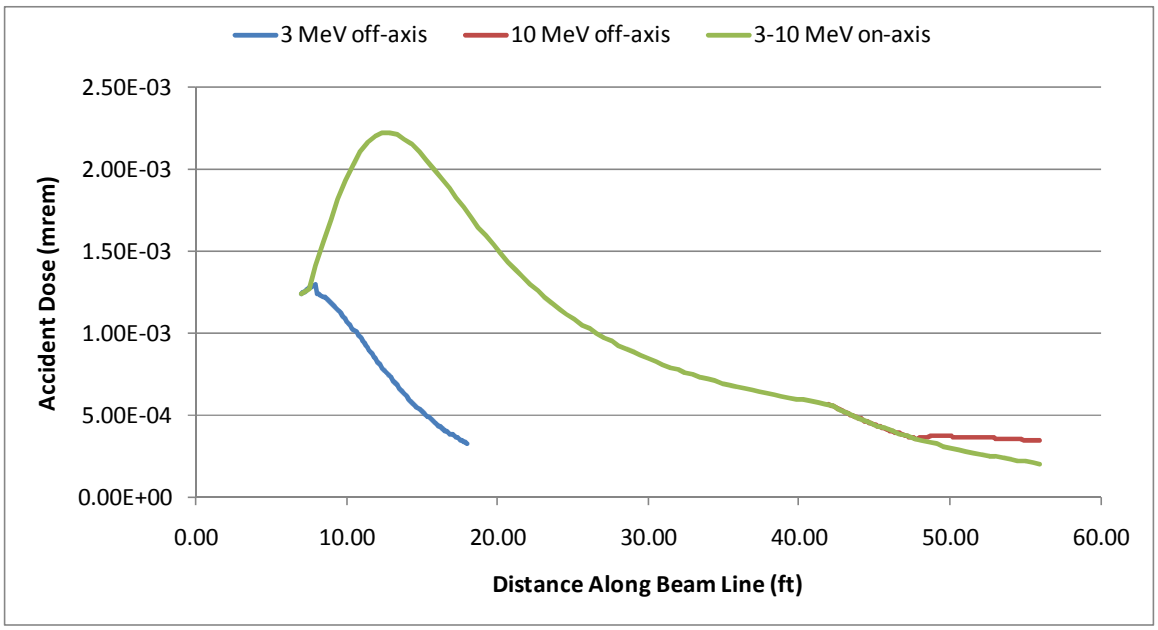

Figure 9: Maximum accident dose outside the south cable penetration versus the location of the loss point.

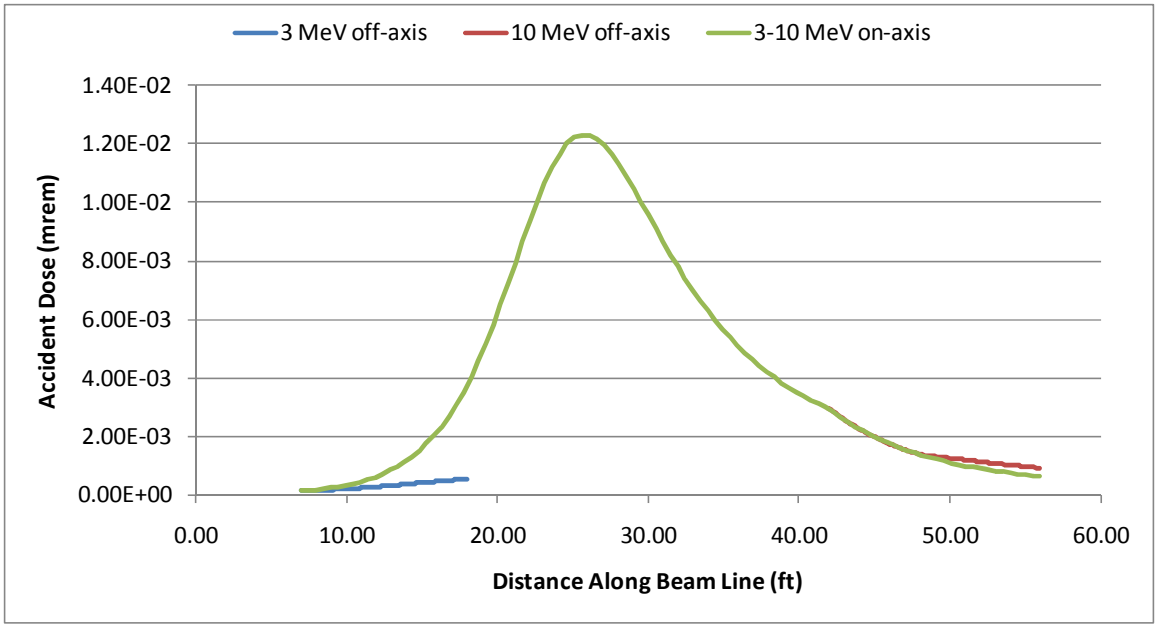

Figure 10: Maximum accident dose outside the middle cable penetration versus the location of the loss point.

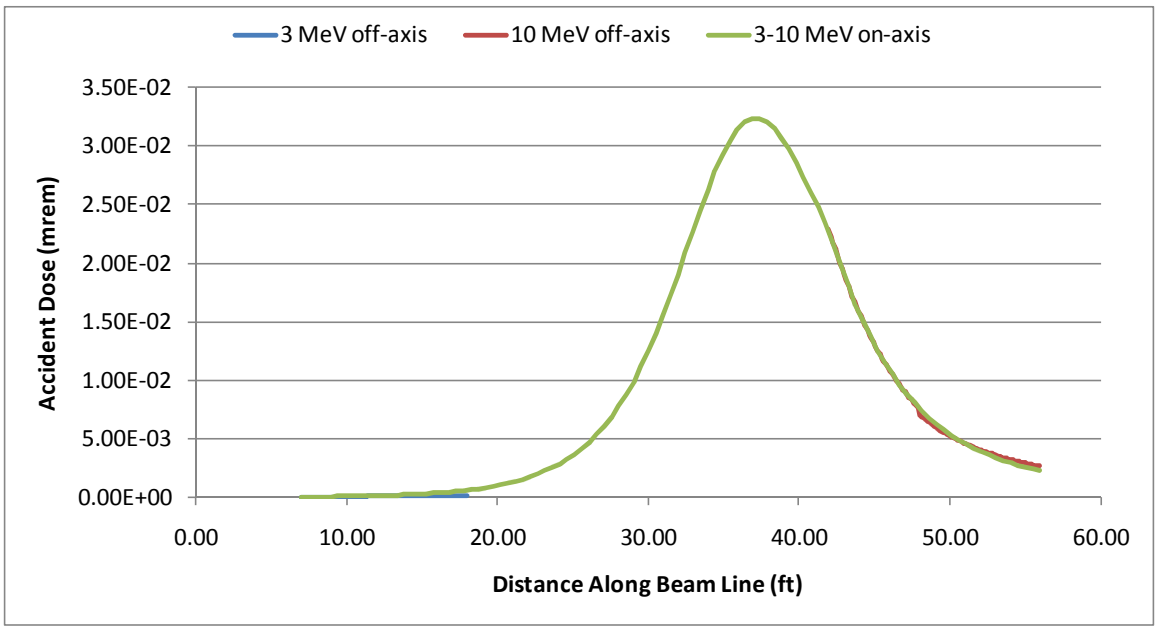

Figure 11: Maximum accident dose outside the north cable penetration versus the location of the loss point.

4.4 Straight Penetrations

There are four straight penetrations into the enclosure that are needed to accommodate a variety of pipes and power bus lines that cannot be readily installed inside a labyrinth. Three of them are 5 ft long but vary in their cross-sectional areas and orientation with respect to the beam direction. The fourth is only 3 ft long but does not face onto any part of the beam lines. Table 11 summarizes the relevant geometric parameters used to in the dose rate calculations.

A square penetration is located along the west wall near the west access labyrinth. This penetration is centered 7.03 ft above the beam line and provides access for several water lines. This penetration will be filled as much as possible with sandbags. The area of the opening without this additional shielding is 2.25 sq. ft.

A large opening in the west wall of the ion-source area is used to provide access for a variety of utilities and is roughly triangular in shape. The opening will be filled as much as possible with hand stacked shielding blocks. The area of the opening without this additional shielding is 12 sq. ft.

The cryogenics penetration is located in the south wall of the enclosure. It is 1.5 ft high and its width varies from 2 to 3 ft. It is used to supply coolants for superconducting devices in the beam line. This penetration enters the enclosure 7.03 ft above the beam line. It will also be filled as much as possible with sandbags. It has 3 sections that are each 1.5 ft long and have cross-sectional areas of 4.5, 3.0, and 3.75 sq. ft. The variable cross-sectional area is dealt with by treating it as the product of three 1.5 ft long straight penetrations.

	Water Penetration	Utility Penetration	Cryogenics Penetration	R.F. Penetration
1st leg length (ft.)	5.00	5.00	1.50	7.50
2nd leg length (ft.)	-	-	1.50	3.00
3rd leg length (ft.)	-	-	1.50	-
1st leg area (sq. ft.)	2.25	12.00	5.25	217.6
2nd leg area (sq. ft.)	-	-	3.00	1.5
3rd leg area (sq. ft.)	-	-	4.50	-
z-location of entrance (ft)	15.75	-17.67	-19.00	-11.00
y-location of entrance (ft)	7.17	12.17	6.17	4.67
x-location of entrance (ft)	7.03	5.53	7.03	0.00

Table 11: Dimensions and locations of the four straight penetrations.

Finally there is a 3.0 x 0.5 ft opening at the top of the northwest wall of the Ion Source & RFQ area that passes through 3 ft of concrete to the roof of the west labyrinth, and is used to bring RF power cables into the enclosure. This penetration is treated as a 2 leg penetration where the 1st leg is formed by the walls of the Ion Source & RFQ Area.

The dose rate calculations for these four penetrations are done using the same methodology that was used for the three-leg penetrations described in the previous sections. However, since these penetrations effectively have only one leg, there are no short-circuit calculations.

Target	Empty Water Penetration	50% Full Water Penetration	Utility Penetration	Cryogenics Penetration	R. F. Penetration
3 MeV off-axis	0.358	0.215	0.023	0.028	1.81E-04
3 MeV on-axis	0.339	0.203	0.028	0.027	4.80E-04
10 MeV off-axis	0.015	8.88E-03	0.037	0.135	0.00
10 MeV on-axis	0.079	0.048	0.063	0.120	6.95E-04

Table 12: Dose rate calculations for the straight penetrations under normal running conditions. The results are given in mrem/hr.

Since it is difficult to assess the effective shielding provided by sandbags, we start by calculating the dose rates expected if the penetrations were empty. The results from the normal operating conditions are presented in Table 12

The dose rate at the outside opening to the water line penetration is predicted to be 0.36 mrem/hr when running 3 MeV into the off-axis absorber at the maximum intensity. This is above the 0.25 mrem/hr limit and hence this configuration is unacceptable without the additional shielding provided by filling the penetration with sandbags.

Rather than try to estimate the amount of attenuation provided by the sandbags we simply varied the effective area of the penetration to determine how carefully the packing needs to be done. We thereby determined that a 50% reduction in the cross-sectional area of the penetration is sufficient to reduce the dose rate sufficiently to meet the FRCM requirements. This should be easily achieved in practice.

The empty penetration calculations for the other penetrations are all below their FRCM limits.

The results of the accident condition calculations are presented in Figure 12 for the water penetration, Figure 13 for the utility penetration, Figure 14 for the cryogenics penetration, and Figure 15 for the RF penetration.

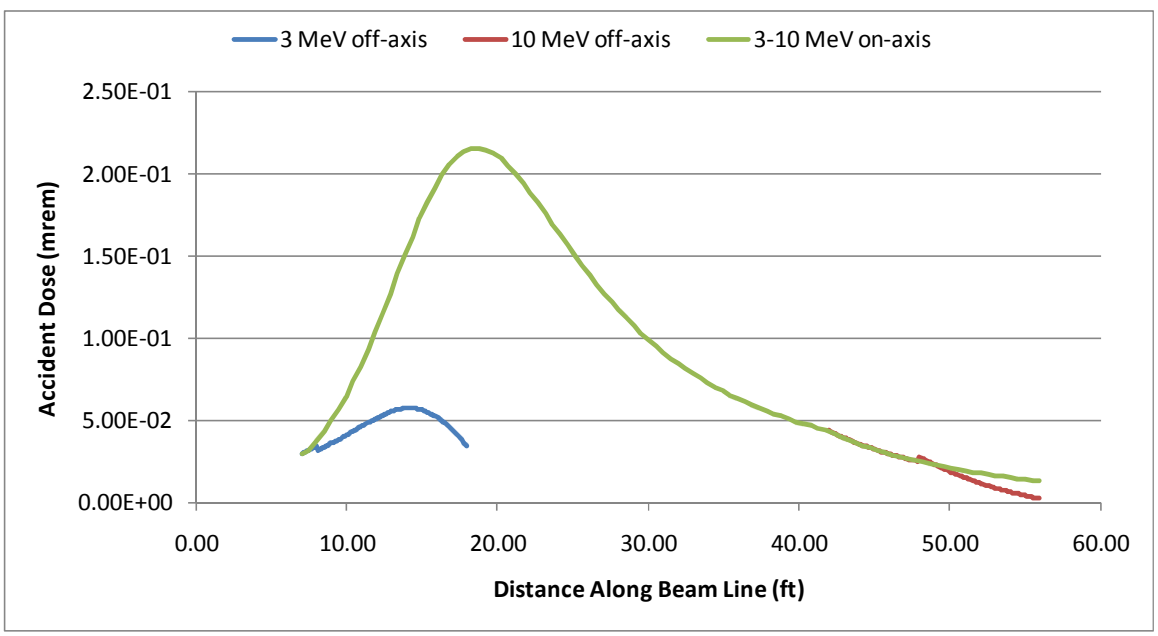

Figure 12: Maximum accident dose outside the water penetration versus the location of the loss point. These doses assume that the opening is 50% full.

The worst case accident occurs when 5 MeV beam is lost in front of the penetration for the water lines. A one second beam loss at that point can produce up to 0.22 mrem at

the outside opening of the penetration. This is the highest accident dose found anywhere in this shielding assessment. Nevertheless, is well below the 5 mrem FRCM.

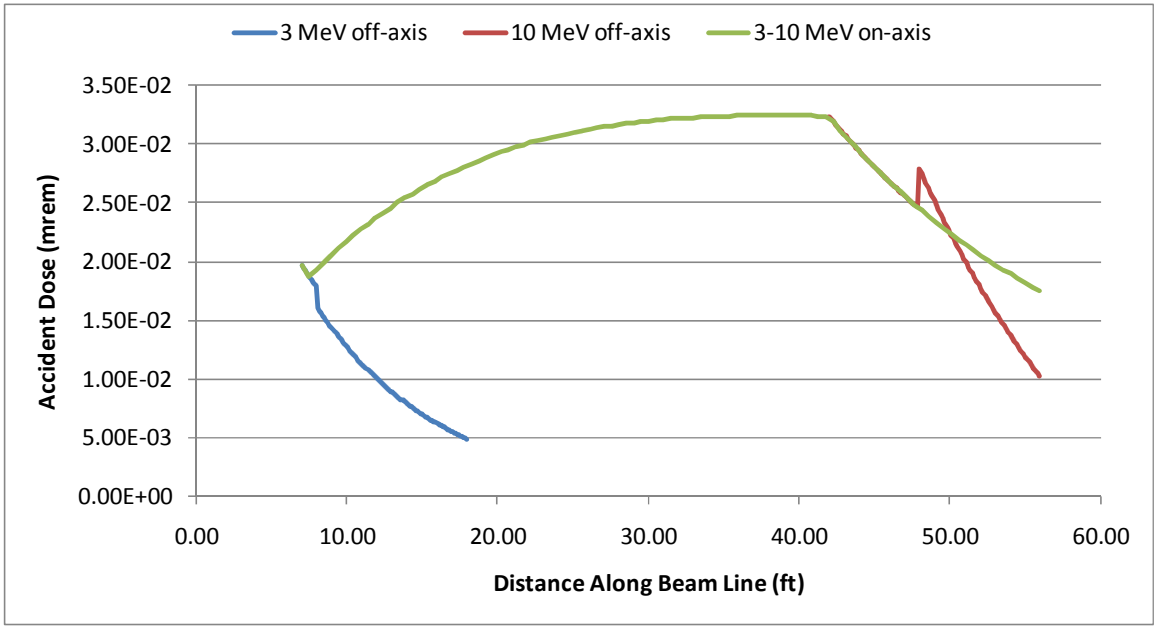

Figure 13: Maximum accident dose outside the utility penetration versus the location of the loss point.

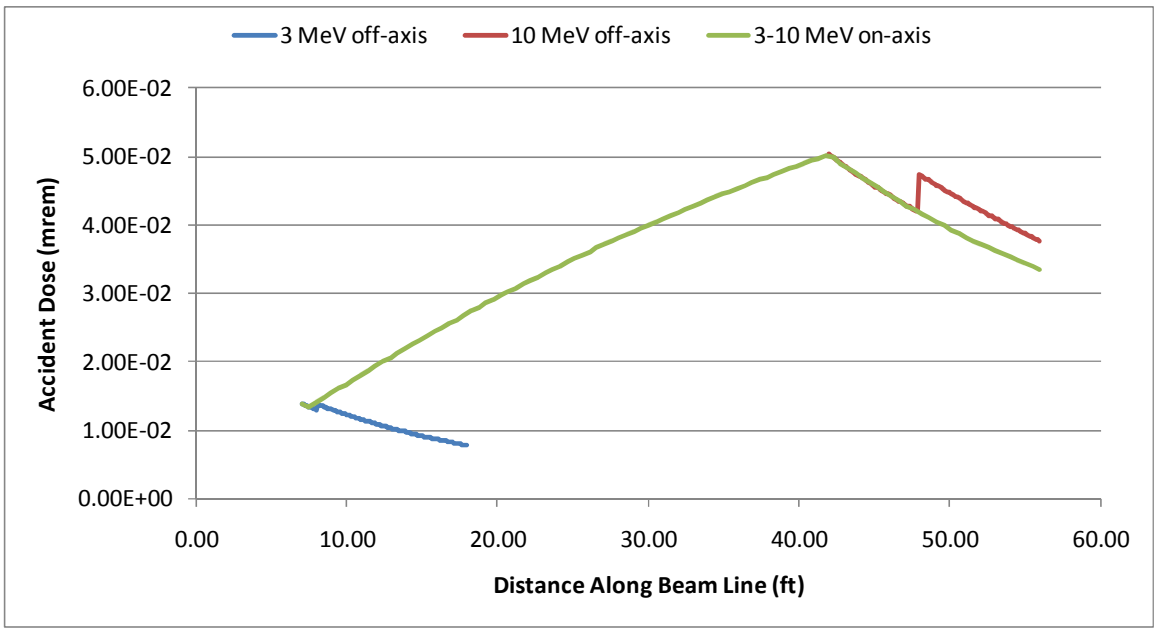

Figure 14: Maximum accident dose outside the cryogenics penetration versus the location of the loss point.

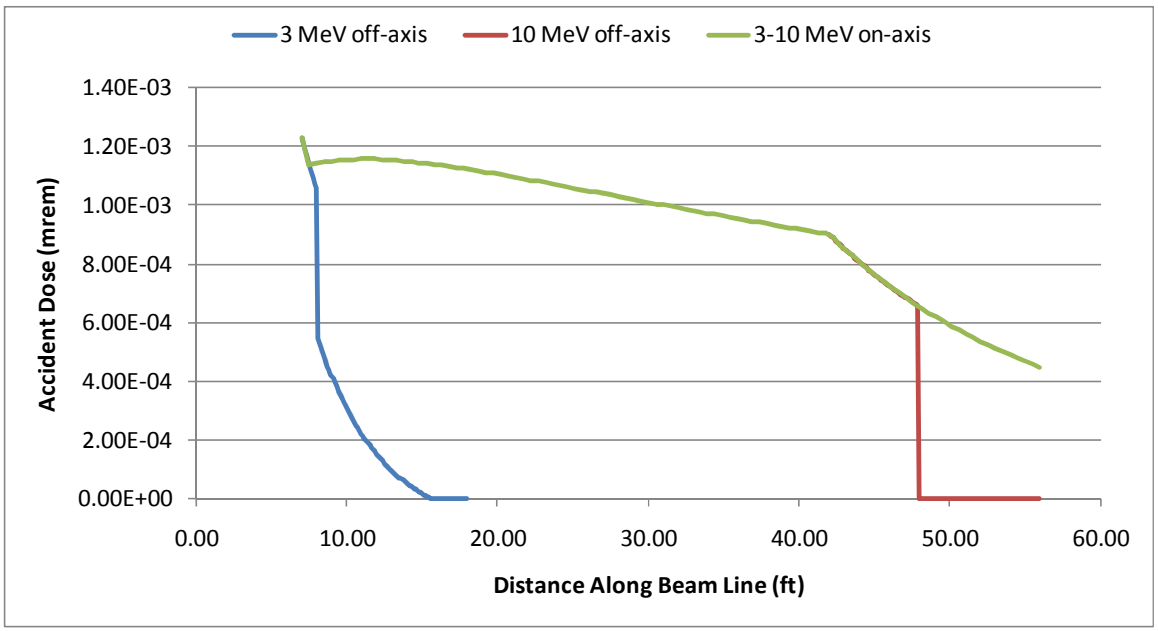

Figure 15: Maximum accident dose outside the RF penetration versus the location of the loss point.

5 Ground and Surface Water Activation

The interaction of protons and neutrons in the soil below the Meson building could produce a variety of radioactive isotopes that can leach into water. The types and concentrations of the isotopes produced, depend on the beam energy and intensity as well as the chemical composition of the soil. The only leachable radionuclides known to be produced in Fermilab soils are ^{3}H, ^{22}Na, ^{45}Ca, and ^{54}Mn. The beam energy thresholds required to produce them ranges from 11 MeV for ^{3}H to 30 MeV for ^{22}Na. Since these thresholds are greater than the maximum beam energy possible with the HINS linac, we conclude that the accelerator is incapable of producing any activated water.

6 Air Activation

The interaction of protons and neutrons with the air inside enclosures can produce airborne radioactive isotopes that can be carried to the site boundary. There is a yearly limit on the amount of activity that can be released off site by the lab as a whole. In this section we show that the 10 MeV linac's contribution to this amount will be negligible.

Under normal conditions the beam line and target will be completely under vacuum so that there will be no direct interactions with the surrounding air. Even if this were not the case, the 10 MeV maximum beam energy is below the neutron production threshold of 11 MeV in nitrogen and 16 MeV in oxygen, which are the two dominant components of air. However, thermal neutrons leaking out of the absorber can produce the radioactive isotope of ^{41}Ar from the naturally occurring ^{40}Ar in the air.

The thermal neutron flux just outside the absorber has been calculated using MARS [3]. The result was 5E+03 /cm^2/s assuming 1.56E+15 protons on target. To obtain a rough estimate of the thermal neutron flux averaged over the entire enclosure, we scale this result by the ratio of the absorber volume (30.3 ft^3) to the enclosure volume (1.6E+04 ft^3) to obtain 6.04E-15 /cm^2/proton. Though this scaling is rather arbitrary, it is also very conservative in that it assumes that the flux calculated by MARS occupies a volume equivalent to size of the absorber.

Knowing the thermal neutron flux, we can use the standard formalism [1] to calculate the amount of air activation expected the production of ^{41}Ar. For the remaining input parameters, we use the values listed below.

- ^{41}Ar production cross section: 660 mbarn
- ^{41}Ar decay constant: 1.05E-04 s^{-1}
- ^{40}Ar concentration in air: 1.25E17 atoms/cc
- Beam-on proton rate: 1.56E15 p/s
- Total protons delivered per year: 2.0E21
- Enclosure air exchange rate: 1 per hour
- Air transit time: 0.5 hr

Under these conditions, we determine that the yearly release of airborne radioactivity will be 0.8 μCi, which is much less than current annual emissions from other parts of the Fermilab site. We also calculate the maximum hourly activation within the enclosure to to be 4.8E-6 pCi/cc which is 0.0005% of the DAC (derived air concentration) defined in Chapter 3 of the FRCM for ^{41}A. Thus no special precautions will be needed for the HINS linac with respect to air activation.

7 Residual Dose Rates

Prolonged exposure to beam can result in a buildup of radioactive isotopes in beam line elements. If the activation levels become large, personnel entering the enclosure when the beam is off may receive radiation doses from these residual sources. In the HINS linac the only beam element that will sustain a prolonged exposure to beam, is the beam absorber.

A MARS simulation [3] was performed to determine the residual dose rates on the outside surface of the beam absorber. This calculation did not include the polyethylene envelope. It was determined that, after 30 days of irradiation at full intensity, followed by a 1 day cool down, the highest residual dose rate was 0.02 mrem/hr at the point where the beam pipe enters the absorber.

The maximum proton energy is below the production threshold of all the radionuclides that can be produced from the interaction of water with 10 MeV protons and its secondaries. The absorber cooling water will not contain any ^{13}N, ^{15}O, ^{11}C or ^{3}H.

8 Controls and Monitoring

In order for the conclusions of this assessment to be valid, the following conditions must be satisfied.

1. Beam will not be enabled if the straight water penetration in the west wall of the linac area has not been filled with sandbags.
2. The beam line and in particular the absorber location must correspond to one of the four configurations considered in this document.
3. Beam will not be enabled without an operational beam interlock safety system.
4. The three labyrinths must be equipped with interlocked gates in order to prevent access into the enclosure while beam is enabled.
5. Radiation detectors must be installed and interlocked to the beam in order to detect any accident conditions and disable the beam within 1 sec.
6. The beam energy shall not exceed 10 MeV.
7. The average beam intensity shall not exceed 6.1E18 protons or H^- ions per hour. (At this intensity the dose rate outside the Water Lines penetration will reach the 0.25 mrem/hr limit)
8. The instantaneous beam intensity shall not exceed 3.3E16 protons or H^- ions per second. (At this intensity the worst case accident condition would generate a dose of 5 mrem outside the Water Lines penetration).
9. Beam monitoring devices, compatible with the Accelerator Division's Beam Budget Monitor, must be installed in order to monitor the beam delivered.

9 Summary & Conclusions

We have analyzed the HINS linac shielding under normal and accident conditions. We have determined that with the controls listed in section **8**, the facility is in conformance with all FRCM requirements and can be operated safely with the following beam parameters.

- Maximum intensity is 6.1E18 protons or H^- ions per hour.
- Maximum energy is 10 MeV.
- Maximum intensity per sec is 3.3E16 protons or H^- ions.

The activation of the air, groundwater, and beam elements is expected to be minimal and imposes no additional constraints on the amount of beam that can be delivered in a year.

10 References

1. "Radiaton Physics for Personnel and Environmental Protection": J. Cossairt, TM1834, (2009).
2. "Fermilab HINS Program 2.5 MeV Beam Design, Operations, and Safety Assessment": R. Webber, ProjectX-doc-520, (2009).
3. "HINS Beam Absorber Mars15 Simulations": N. Mokhov, Beams-doc-3597, (2010).
4. "A Guide to Radiation and Radioactivity Levels Near High Energy Particle Accelerators": A. H. Sullivan, Nuclear Technology Publishing, (1992).
5. "Incremental Shielding Assessment Methodology": W. Higgins & P. Kasper, (1997)
6. "Fermilab Radiological Control Manual": Section 2.3, (2010).